JOURNAL OF
THE ENGINEERING
MECHANICS DIVISION

CREEP AND SHRINKAGE LAW FOR CONCRETE AT VARIABLE HUMIDITY

By Zdeněk P. Bažant,[1] M. ASCE and Spencer T. Wu[2]

INTRODUCTION

Structural analysis with complex constitutive laws has been made feasible by electronic computers, but for many materials realistic constitutive laws themselves are unavailable at present. This is certainly true in the case of creep and shrinkage of concrete at variable humidity. An experimentalist may point out that better controlled and better designed experiments are needed to enhance the knowledge. Yet, this is only a part of the answer. Perusing the literature, one cannot deny that a vast pool of experimental information already exists, but it remains largely untapped as far as the quantitative theoretical model is concerned. Although numerous studies have been devoted to moisture effects in concrete, no consistent constitutive law for concrete creep and shrinkage at variable humidity has yet been identified from the test data, to the best of writers' knowledge, and this task is chosen as the object of this study.

The problem is made difficult partly by the fact that the standard test specimens are during the test in a nonhomogeneous state, i.e., in a state of nonuniform stress, strain, and pore humidity. Mathematically, one faces a so-called inverse problem, because coefficients of a differential equation in space and time must be identified from a given solution, the measured data. Such problems have been studied extensively in the theories of control and optimization and became tractable only recently with the help of a computer. Application of these techniques can greatly improve the understanding of concrete behavior and should be begun on a large scale because it would be even more fruitful (and less costly) than further testing until all available experimental data are theoretically analyzed.

Apart from the identification problem, an even more complex problem is

Note.—Discussion open until May 1, 1975. To extend the closing date one month, a written request must be filed with the Editor of Technical Publications, ASCE. This paper is part of the copyrighted Journal of the Engineering Mechanics Division, Proceedings of the American Society of Civil Engineers, Vol. 100, No. EM6, December, 1974. Manuscript was submitted for review for possible publication on March 6, 1974.

[1]Prof. of Civ. Engrg., Northwestern Univ., Evanston, Ill.

[2]Sr. Engrg. Analyst, Sargent & Lundy, Engrs., Chicago, Ill.; formerly, Grad. Research Asst., Northwestern Univ., Evanston, Ill.

perhaps that of the choice of the proper form of the constitutive equation. Here, a thermodynamic theory of the microstructural creep mechanism has proven to be quite helpful and has led to a rational form of the constitutive law (1,3,4,6). The present study attempts to determine quantitatively the material parameters of this law.

A constitutive equation that is formulated in relationship to the underlying physical processes in the microstructure inevitably has a rate-type form with hidden (internal) variables. Fortunately, this form is, at the same time, particularly expedient because it eliminates the history dependence. Indeed, for the analysis of large structural systems a rate-type form is inevitable, because the storage of all stress values in all previous time steps and the evaluation of hereditary integrals, as required by an integral-type law, would make the computer storage and time requirements prohibitively large. Special cases of the constitutive equation to be considered herein have been studied quantitatively for the cases of constant humidity and both constant and variable temperature already in Refs. 9 and 10, and a different but analogous formulation was given in Ref. 8. The present study is a continuation of these works.

Constitutive Law and Its Relation to Thermodynamics of Creep Mechanism

On the microstructural level, the creep in portland cement concrete and a major part of its shrinkage are almost certainly caused by a diffusion flux of a certain component forming the solid particles [probably Ca ions (4,6)] coupled with diffusion fluxes of water along the hindered adsorbed layers in cement gel (4,6). This contemporaneous concept of the creep mechanism is essentially an extension and modification of the ideas of Powers (26,27) on the disjoining pressure in hindered adsorbed layers and has been developed chiefly in Refs. 3 and 6. Under certain plausible assumptions, the mathematical formulation of this mechanism leads, for hydrostatic stress states and constant temperature, to a constitutive equation of the form (see Eq. 4.30 in Ref. 4):

$$\dot{\sigma}^V_{s_\mu} + \phi^V_{ss_\mu}\sigma^V_{s_\mu} + \phi^V_{sw_\mu}(\sigma^V_{w_\mu} - \sigma^h_\mu) = 3K^s_\mu[\dot{\epsilon}^V - \dot{\epsilon}_S(h)] \quad \ldots\ldots\ldots (1a)$$

$$\dot{\sigma}^V_{w_\mu} + \phi^V_{ws_\mu}\sigma^V_{s_\mu} + \phi^V_{ww_\mu}(\sigma^V_{w_\mu} - \sigma^h_\mu) = 3K^w_\mu[\dot{\epsilon}^V - \dot{\epsilon}_S(h)] \quad \ldots\ldots\ldots (1b)$$

$$\sum_\mu (\sigma^V_{s_\mu} + \sigma^V_{w_\mu}) = \sigma^V; \quad \mu = 1, 2, \ldots, n \quad \ldots\ldots\ldots\ldots\ldots\ldots (2)$$

in which ϵ^V, σ^V = volumetric strain and stress; superscript V refers to volumetric component; $\sigma^V_{s_\mu}, \sigma^V_{w_\mu}$ = hidden volumetric stresses in solids (subscript s) and in water (subscript w); K^s_μ, K^w_μ = (tangent) elastic bulk moduli of solids and water associated with the hidden stresses; $\epsilon_S(h)$ = instantaneous shrinkage strain depending on the relative humidity, h, in the capillary pores (macropores) within the material; $\phi^V_{ss_\mu}, \phi^V_{sw_\mu}, \phi^V_{ws_\mu}, \phi^V_{ww_\mu}$ = rate coefficients associated with the microscopic diffusion fluxes of solids (s) and water (w), and their mutual coupling; σ^h_μ = functions of h = values of hidden stresses in hindered adsorbed water layers that would be necessary for thermodynamic equilibrium with the adjacent capillary pores containing water vapor of humidity h (see Ref. 4); zero value of σ^h_μ is chosen at $h = 1$; and the dots refer to the derivatives with respect to time t; e.g., $\dot{\epsilon} = d\epsilon/dt$. Eqs. 1$a$, 1$b$, and 2 can be applied only for the stress range in which microcracking is negligible, i.e., when stresses are less

than about one-half of the strength. The coefficients of Eqs. 1 and 2 may be expressed in terms of the parameters and thermodynamic variables of the microstructural model (see Ref. 4, Eqs. 4.21–4.24).

If the material is assumed to be isotropic, the deviatoric strain rates must be independent of the volumetric strain rates and must be governed by a constitutive equation of similar form but devoid of stress-independent terms, such as σ^h_μ and ϵ_S. Thus

$$\dot{\underset{\sim}{\sigma}}^D_{s_\mu} + \phi^D_{ss_\mu}\underset{\sim}{\sigma}^D_{s_\mu} + \phi^D_{sw_\mu}\underset{\sim}{\sigma}^D_{s_\mu} = 2G^s_\mu\dot{\underset{\sim}{\epsilon}}^D \quad \ldots\ldots\ldots\ldots\ldots\ldots (3a)$$

$$\dot{\underset{\sim}{\sigma}}^D_{w_\mu} + \phi^D_{ws_\mu}\underset{\sim}{\sigma}^D_{s_\mu} + \phi^D_{ww_\mu}\underset{\sim}{\sigma}^D_{w_\mu} = 2G^w_\mu\dot{\underset{\sim}{\epsilon}}^D \quad \ldots\ldots\ldots\ldots\ldots\ldots (3b)$$

$$\sum_\mu (\underset{\sim}{\sigma}^D_{s_\mu} + \underset{\sim}{\sigma}^d_{w_\mu}) = \underset{\sim}{\sigma}^D; \quad \mu = 1, 2, \ldots, n \quad \ldots\ldots\ldots\ldots\ldots\ldots (4)$$

in which $\underset{\sim}{\sigma}^D = [\sigma^D_{ij}] = [\sigma_{ij}] - \sigma^V[\delta_{ij}]$ = deviatoric stress tensor; $\underset{\sim}{\epsilon}^D = [\epsilon^D_{ij}] = [\epsilon_{ij}] - \epsilon^V[\delta_{ij}]$ = deviatoric strain tensor; $\underset{\sim}{\sigma} = [\sigma_{ij}]$ = stress tensor; $\underset{\sim}{\epsilon} = [\epsilon_{ij}]$ = strain tensor; i, j = subscripts for cartesian coordinates x_i, $i = 1, 2, 3$; δ_{ij} = Kronecker delta; $\underset{\sim}{\sigma}^D_{s_\mu}, \underset{\sim}{\sigma}^D_{w_\mu}$ = similarly defined deviatoric tensors of hidden stresses in solids (s) and water (w); $\phi^D_{ss_\mu}, \phi^D_{sw_\mu}, \phi^D_{ws_\mu}, \phi^D_{ww_\mu}$ = rate coefficients; and G^s_μ, G^w_μ = (tangent) elastic shear moduli (of solids and hindered adsorbed water), associated with the hidden stresses.

Analysis of Constitutive Equation

According to Eqs. 2 and 4, the (macroscopic) stress is assumed to be a resultant of all hidden stresses. This means that the constitutive equation may be visualized by means of a Maxwell-type chain, shown in Fig. 1(a), in which the layer-shaped "diffusion elements" are characterized by rate coefficients $\phi^V_{ss_\mu}$, ... or $\phi^D_{ss_\mu}$, ..., the springs model the instantaneous response of solids and (hindered adsorbed) water, and ϵ_S is superimposed on the deformation of the model in the volumetric case.

The Maxwell chain model, consisting of dashpots and springs of age-dependent moduli, that was previously developed for the rate-type creep law of aging concrete at $h \approx 1$ and reference temperature T_0 (the reference conditions), is a special case of the present model (5,9). Indeed, adding Eqs. 1a and 1b (and noting that $\sigma^h_\mu = \dot{\epsilon}_S = 0$ at $h = 1$) one can see that the well-known relations for a spring-dashpot Maxwell chain [Fig. 1(b)]:

$$\sigma^V = \sum_\mu \sigma^V_\mu, \quad \frac{\dot{\sigma}^V_\mu}{3K_\mu(t)} + \frac{\sigma^V_\mu}{3\eta_\mu(t)} = \dot{\epsilon}^V; \quad \mu = 1, 2, \ldots, n \quad \ldots\ldots\ldots\ldots (5)$$

are a special case of Eqs. 1 and 2, provided that

$$\phi^V_{ss_\mu} + \phi^V_{ws_\mu} = \phi^V_{sw_\mu} + \phi^V_{ww_\mu} = \frac{K_\mu(t)}{\eta_\mu(t)} = \frac{1}{\tau_\mu} \quad \ldots\ldots\ldots\ldots\ldots\ldots (6)$$

$$K^s_\mu + K^w_\mu = K_\mu(t); \quad \sigma^V_{s_\mu} + \sigma^V_{w_\mu} = \sigma^V_\mu \quad \ldots\ldots\ldots\ldots\ldots\ldots (7)$$

in which σ^V_μ = volumetric total hidden stresses; $K_\mu(t)$ = total bulk modulus at age t corresponding to σ^V_μ; $\eta_\mu(t)$ = (dashpot) viscosity at age t; and τ_μ

= relaxation time associated with σ_μ^V. Similar relations can be obtained from Eq. 3 for the deviatoric components.

The question whether a chain of the Maxwell type or of the Kelvin type should be considered is in classical viscoelasticity solely a matter of choice because either of these two chains can approximate any viscoelastic behavior with any desired accuracy. This also holds in the case of time-variable (aging) materials, e.g., concrete, but the Maxwell chain is preferrable for two reasons: (1) Its differential equations (8,9) are of the first order in ϵ while those for

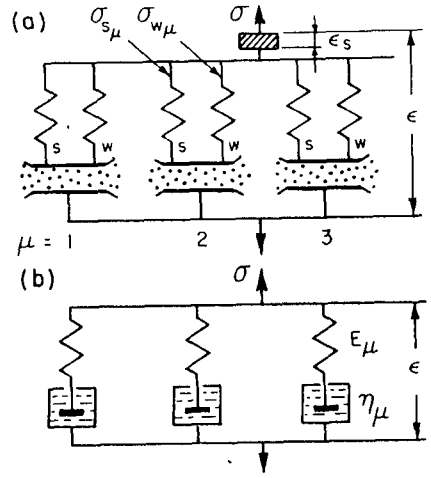

FIG. 1.—(a) Model Interpreting Structure of Constitutive Equation at Variable Humidity; (b) Maxwell Chain Model as Special Case

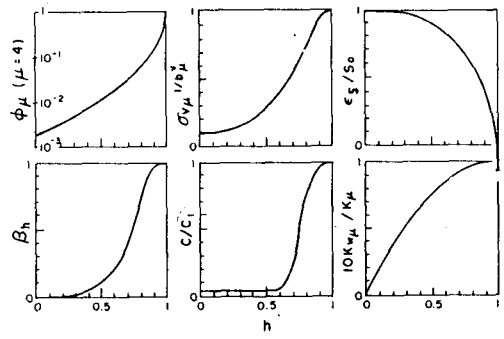

FIG. 2.—Dependence of Various Material Parameters on Pore Humidity h

the Kelvin chain are of the second order in ϵ (though of first order in $\dot{\epsilon}$) and this somewhat complicates the integration; and (2) when the physical interpretation in terms of hindered adsorbed layers is considered, it is more appropriate to superimpose the stresses in solids and water than the strains in solids and water, and this condition is satisfied only by the Maxwell chain.

Identification of the material parameters of Eqs. 5-7 for the case of reference

conditions ($h = 1$, $T = T_0$) is the first problem to be tackled. It has already been resolved; see Ref. 9 with the computer program listed in Ref. 5. Moduli $K_\mu(t)$ may be regarded as functions of $\log \tau_\mu$, and the plot of $K_\mu(t)$ versus $\log \tau_\mu$ at fixed time t is called the relaxation spectrum. This spectrum is discrete and is actually an approximation of a certain continuous spectrum. Obviously, for a discrete approximation of a continuous function, different choices of discrete coordinate values may give equally good approximations. Thus, the $\log \tau_\mu$ values may be chosen in advance arbitrarily, provided that they are sufficiently densely distributed and cover the whole time range of interest. (In fact, it is impossible to attempt determination of τ_μ from test data, because a problem with a nonunique solution and an unstable dependence of τ_μ on the data would result.) It is most convenient to select $\tau_\mu = \eta_\mu(t)/K_\mu(t)$ to be independent of age t, constraining thus $\eta_\mu(t)$ and $K_\mu(t)$ to vary proportionately (see Refs. 9 and 10). Further, a suitable choice is a set of τ_μ values distributed uniformly on the logarithmic scale, i.e., $\tau_\mu = \tau_1 a^{\mu-1}$. For applications in structural analysis, the number, n, of hidden stresses should be kept to a minimum. A sufficient accuracy is achieved with $a = 10$, i.e.

$$\tau_\mu = \tau_1 10^{\mu-1}; \quad \mu = 1, 2, \ldots, n \quad \ldots\ldots\ldots\ldots\ldots\ldots\ldots\ldots (8)$$

After specifying the values of τ_μ, one can determine moduli $K_\mu(t')$ for age t' by expanding the relaxation curve for constant stress applied at age t' in a series of real exponentials, called Dirichlet series (8,9); this is best done by the method of least squares. (The relaxation curve can be obtained from a set of creep curves for various ages at loading by solving a Volterra integral equation numerically (9); also see the computer program in Ref. 5.) However, for τ_μ values spaced too closely, moduli K_μ are unstable functions of the test data, i.e., quite different K_μ values can give equally close fits. This is true even of the spacing in Eq. 8. Nevertheless it was found (8) that this unacceptable feature can be avoided by including into the least-square condition of optimum fit a penalty term of the form $\Sigma_\mu [w_1(K_{\mu+1} - K_\mu)^2 + w_2(K_{\mu+2} - 2K_{\mu+1} + K_\mu)^2]$, with w_1 and w_2 being suitable weight factors. This forces K_μ to be a "smooth" function of μ, which is physically a natural property to require.

The preceding analysis evidently applies not only for the volumetric behavior, but also for the deviatoric behavior.

In similarity with relaxation times τ_μ, and because of Eq. 6, it is necessary to choose the rate coefficients. An expedient choice is

$$\phi^V_{ss_\mu} = \phi^V_{ww_\mu} = \phi^D_{ss_\mu} = \phi^D_{ww_\mu} = \frac{k_\mu}{\tau_\mu}; \quad \phi^V_{sw_\mu} = \ldots = \phi^D_{sw_\mu} = \frac{1 - k_\mu}{\tau_\mu}; \quad \text{at } h = 1 \quad (9)$$

This choice ensures that Eq. 6 is satisfied and implies that a significant coupling, characterized by $\phi^V_{sw_\mu}$, ..., can exist only between diffusion processes having a rate that is of the same order of magnitude. Physically, this assumption seems to be a reasonable one because diffusion is a rate process without memory. (According to Eq. 12 in the sequel, $k_\mu = 1$.)

The present constitutive equations differ from those of viscoelasticity primarily by the fact that hidden stresses σ_μ are split into two independent components, σ_{s_μ} and σ_{w_μ}, due to solids and hindered adsorbed water. One reason for this splitting relates to the processes in the microstructure (see Sections 4.4 and

4.5 in Ref. 4), and two further reasons exist: (1) A separate parameter for the state of water in the hindered adsorbed layers is necessary to model that part of shrinkage that is delayed with regard to pore humidity change; and (2) creep at constant h depends on stress (up to about 0.4 of the strength) nearly linearly, while creep during drying depends upon stress distinctly nonlinearly (20,21,34). Because the time-dependent deformations are caused primarily by the diffusion of solids rather than water (as shown in Ref. 4), the law of solids diffusion must be essentially linear and the coupling between the diffusion of water and the diffusion of solids must be nonlinear. To model these two distinct time-dependent processes, two separate variables, σ_{s_μ} and σ_{w_μ}, evidently are needed. (In the sequel, the nonlinear coupling is modeled by coefficients ψ_μ^V and ψ_μ^S).

Another important difference from the classical viscoelasticity is the presence of terms σ_μ^h. They depend on pore humidity h and represent the values that σ_{w_μ} must have in thermodynamic equilibrium with water vapor of humidity h in the macropores. Consequently, they are additive to $-\sigma_{w_\mu}$ and are multiplied by the same rate coefficient, expressing the fact that creep and shrinkage are merely different facets of the same physical phenomenon. Terms σ_μ^h cause those stress-independent humidity-dependent deformations (i.e., shrinkage) that occur with a certain delay after a change of humidity h in the capillary pores. The fitting of various data, as well as direct evidence (11), confirmed that the delayed shrinkage is of the same order of magnitue as the instantaneous shrinkage, modeled by the term, ϵ_S, in Eq. 1.

Material Parameters.—Using the methods outlined subsequently, the dependence of the material parameters upon pore humidity, progress of hydration, relaxation time, and stress has been identified as shown in the following. The rate coefficients are expressed as:

$$\phi_{ss_\mu}^V = \frac{1}{\tau_\mu}\phi_\mu\psi_\mu^V\rho_\mu^V;\quad \phi_{ww_\mu}^V = \frac{1}{\tau_\mu}\phi_\mu\psi_\mu^V \quad \ldots\ldots (10)$$

$$\phi_{ss_\mu}^D = \frac{1}{\tau_\mu}\phi_\mu\psi_\mu^D\rho_\mu^D;\quad \phi_{ww_\mu}^D = \frac{1}{\tau_\mu}\phi_\mu\psi_\mu^D \quad \ldots\ldots (11)$$

$$\phi_{sw_\mu}^V = \phi_{ws_\mu}^V = \phi_{sw_\mu}^D = \phi_{ws_\mu}^D \approx 0;\quad \tau_\mu = 0.05 \times 10^{\mu-1}\ \text{days};$$

$$\mu = 1, \ldots, n;\quad n = 7 \quad \ldots\ldots (12)$$

in which $\phi_\mu = \psi_\mu^V = \rho_\mu^V = \psi_\mu^D = \rho_\mu^D = 1$ for $h = 1$ and very small stress, while for general h and a higher stress (see Fig. 2):

$$\phi_\mu = 10^{-a_\mu\sqrt{1-h}};\quad \psi_\mu^V = 1 + \left(\frac{\sigma_{w_\mu}^V - \sigma_\mu^h}{\sigma_{V_\mu}}\right)^2;\quad \psi_\mu^D = 1 + \left(\frac{\sigma_{w_\mu}^V - \sigma_\mu^h}{\sigma_{D_\mu}}\right)^2 \quad (13)$$

$$\rho_\mu^V = \rho_\mu^D = 1 + \left(\frac{\sigma_{s_\mu}^V}{\sigma_{a_\mu}}\right)^2 + \frac{J_2(\underset{\sim}{\sigma}_{s_\mu}^D)}{\sigma_{b_\mu}^2} \quad \ldots\ldots (14)$$

in which $\sigma_{V_\mu} = 10^{-b_\mu^V(1-h^2)^2}\sigma_C$; $\sigma_{D_\mu} = 10^{-b_\mu^D(1-h^2)^2}\sigma_C$;

$$a_\mu = 3.6 - 0.095(\mu - 1)^2;\quad \sigma_C = 0.0414\ \text{N/mm}^2\ (6\ \text{psi}) \quad \ldots\ldots (15)$$

$$b_\mu^D = 0.3 \times 10^{B_\mu};\quad b_\mu^V = 1.2\,b_\mu^D;\quad B_\mu = 1.4 + \beta(\mu - 1) \quad \ldots\ldots (16)$$

$$\sigma_{b_\mu} = \sigma_{a_\mu} = (1.1 + 0.2\mu)\sigma_B;\quad \sigma_B = 0.006895\ \text{N/mm}^2\ (1\ \text{psi}) \quad \ldots\ldots (17)$$

and $J_2(\underset{\sim}{\sigma}_{s_\mu})$ = second invariant of the deviatoric tensor, $\underset{\sim}{\sigma}_{s_\mu}^D$. The terms causing shrinkage are (see Fig. 2):

$$\epsilon_S = S_0(1 - 0.95h^3 - 0.25h^{200}) \quad \ldots\ldots (18)$$

$$\sigma_\mu^h = S_1\frac{\tau_S}{\tau_S + \tau_\mu}\frac{\epsilon_S}{S_0};\quad \tau_S = 20\ \text{days} \quad \ldots\ldots (19)$$

The (tangent) elastic moduli are expressed as

$$K_{s_\mu} = 0.9\,K_\mu;\quad K_{w_\mu} = 0.1h(2 - h)\,K_\mu;\quad G_{s_\mu} = 0.9\,G_\mu;$$
$$G_{w_\mu} = 0.1h(2 - h)\,G_\mu \quad \ldots\ldots (20)$$

$$G_\mu = \frac{E_\mu(t_e)}{2(1+\nu)};\quad K_\mu = \frac{E_\mu(t_e)}{3(1-2\nu)};\quad \nu \approx 0.18 \quad \ldots\ldots (21)$$

$$E_\mu(t_e) = E_{0_\mu} + E_{1_\mu}t_e^{1/8} + E_{2_\mu}t_e^{1/4} + E_{3_\mu}t_e^{1/2} + E_{4_\mu}t_e^{3/4} \quad \ldots\ldots (22)$$

in which ν is the Poisson ratio for elastic deformation and creep at $h = 1$ and is known to be nearly independent of creep duration and age; $\nu \approx 0.18$ (4,24). Parameters $E_{0_\mu}, \ldots, E_{4_\mu}$ can be determined from the uniaxial creep compliance function, $J(t, t')$, by a program listed in Ref. 5. t_e is the equivalent hydration period, defined (7) at constant temperature as (see Fig. 2):

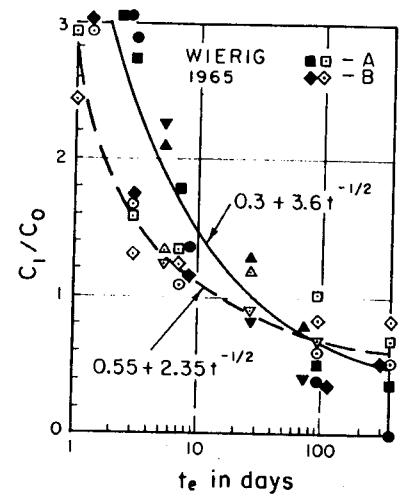

FIG. 3.—Comparison of Eq. 26 with Wierig's Data (3) on Water Vapor Permeability [t_e = **curing period** t_e **in water. Approximately** $C_1 \sim c$. **Measured at 20° C on slabs 15 mm thick; one surface exposed to humidity 0%, the other to 95% (empty points) or to 50% (solid points); unit ordinate corresponds to** 33×10^{-9} **kg m/kgf hour for 50%, or to** 66×10^{-9} **for 95%; A = ordinary cement; B = high early strength cement, the rest = low-heat late-set cements.**]

$$t_e = \int_0^t \beta_h \, dt; \quad \text{with} \quad \beta_h = [1 + (3.5 - 3.5h)^4]^{-1} \quad \ldots\ldots\ldots\ldots \quad (23)$$

Despite the restriction to working stress range, nonlinear behavior may occur in tension. This must be considered when the test data on shrinkage are analyzed. It is assumed that for uniaxial tensile stress σ and strain ϵ the instantaneous

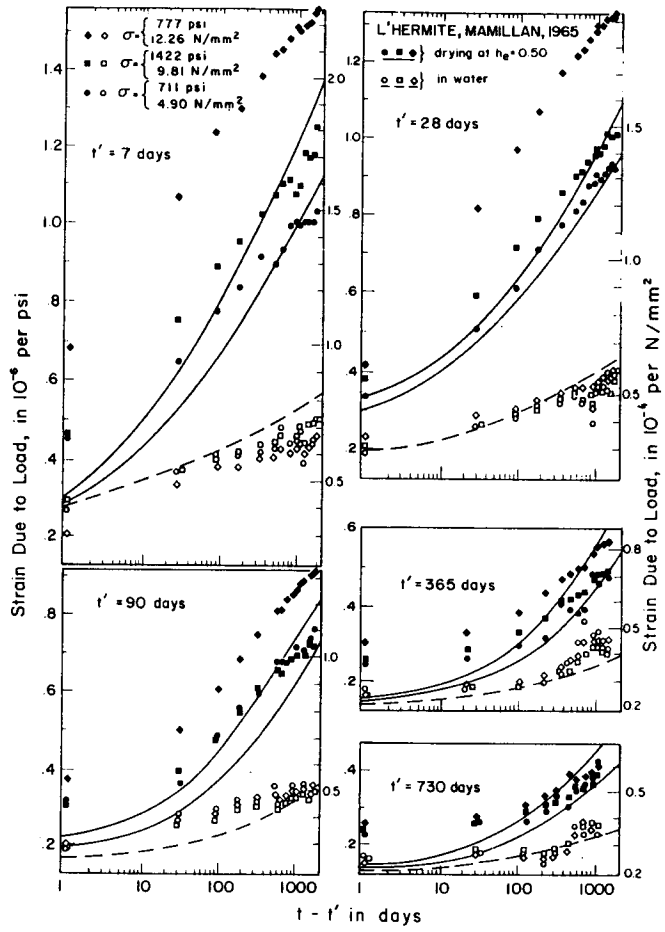

FIG. 4.—Fits of L'Hermite and Mamillan's Uniaxial Compression Creep Data (20) [t' = age at loading; prisms 7 cm × 7 cm × 28 cm approximated as 7.5-cm diam. cylinders; 28-day strength = 35.9 N/mm² (5,200 psi); room temperature; concrete of French type 400/800; 350 kg cement/m³; water-cement-sand-gravel ratio = 0.49: 1: 1.75: 3.07; Seine gravel. Measured J values at $t - t' \approx 0.01$ day for ages t' = 7 days to 730 days shown were 248, 196, 190, 172, 144 in 10^{-9}/psi (14.5 × 10^{-6} per N/mm²). Drying exposure began at age t_0 = 2 days. Fits for f'_t = 2.76 N/mm² (600 psi), S_1 = 1.70 N/mm² (260 psi), S_0 = 0.0003, C_0 = 0.161 cm²/day (0.025 sq in./day), B = 0.4. Data points for 12.26 N/mm² (1,777 psi) are not fitted since they are in high stress range.]

$\sigma - \epsilon$ diagram is of the Ramberg-Osgood type, i.e., $\epsilon = \sigma/E + (2f'_t/E)(\sigma/f'_t)^3$, in which f'_t = failure stress in tension. Accordingly, the tangent elastic modulus in tension is $E_{tan} = E/(1 + 6\sigma^2/f'^2_t)$. Assuming that moduli $E_\mu(t_e)$ depend on maximum principal tensile stress σ_t similarly as E_{tan} depends on σ, all $E_\mu(t_e)$ must be replaced by

$$\frac{E_\mu(t_e)}{1 + \dfrac{6\sigma_t^2}{f'^2_t}} \quad \ldots\ldots\ldots\ldots\ldots\ldots\ldots\ldots\ldots\ldots\ldots\ldots \quad (24)$$

When σ_t reaches f'_t, a macroscopic crack is formed and the stress drops to 0.

To determine pore humidity h, the macroscopic water diffusion through concrete must be analyzed. Fortunately, it has been found that as a very good approximation this problem may be considered independent of the deformations. Diffusivity

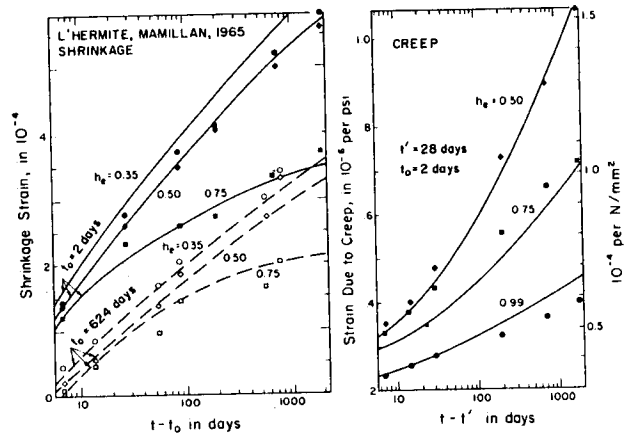

FIG. 5.—Fits of L'Hermite and Mamillan's Creep and Shrinkage Data (20) at Various Humidities (Same Parameters as in Fig. 4.)

C in the diffusion equation for h depends strongly upon h (7); approximately (see Fig. 2):

$$C = C_1(t_e)\left[0.05 + \frac{0.95}{1 + (4 - 4h)^6}\right] \quad \ldots\ldots\ldots\ldots\ldots\ldots \quad (25)$$

By fitting Wierig's data (31) on vapor permeability c, which is approximately proportional to C, it has been found (see Fig. 3) that

$$C_1 = C_0(0.3 + 3.6\, t_e^{-1/2}), \quad \text{or} \quad C_0(0.55 + 2.35\, t_e^{-1/2}) \quad \ldots\ldots\ldots\ldots \quad (26)$$

in which the first expression applies to regular (type I) cements and the second applies to early strength (type III) cements. The diffusion equation for h also contains term h_s due to self-desiccation of sealed concrete caused by hydration. It may be expressed (for water-cement ratios of about 0.45) as

$$h_s(t_e) = \frac{0.98t_e + \tau_s}{t_e + \tau_s}; \quad \tau_s = 20 \text{ days} \quad \ldots\ldots\ldots\ldots\ldots\ldots\ldots\ldots\ldots (27)$$

The finite rate of moisture transmission at the exposed surface of the concrete has been handled (7) in terms of the equivalent surface thickness, D_h, which has been considered to be 1.25 mm for all test data analyzed.

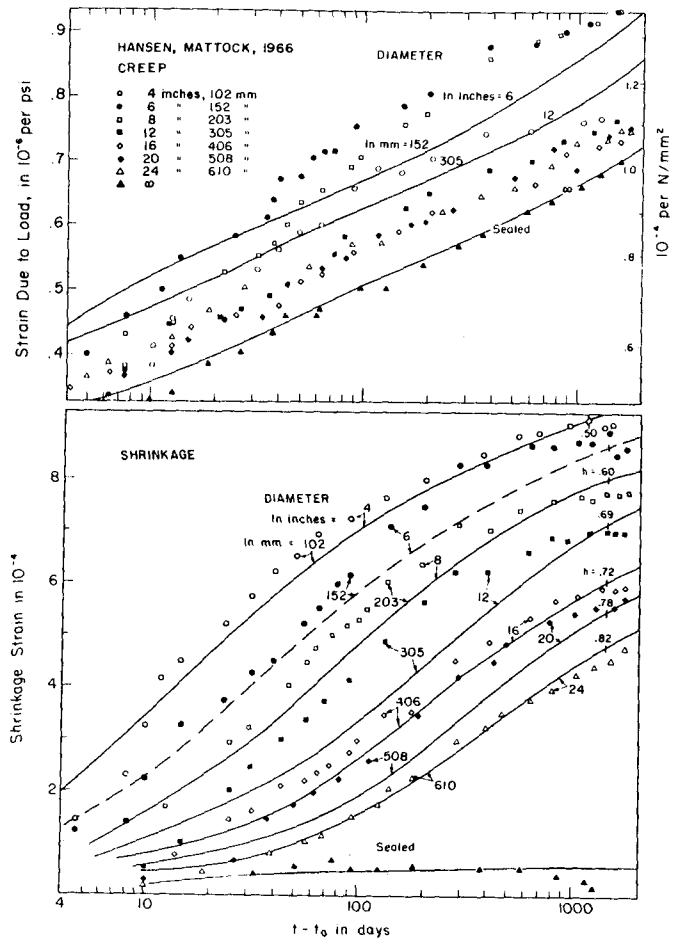

FIG. 6.—Fits of Hansen and Mattock's data (17) on Effect of Size on Shrinkage and Creep of Cylinders Drying at $h_e = 0.50$ [Cylinders sealed at ends; 28-day cylinder strength ≈ 41.4 N/mm² (6,000 psi); Elgin gravel (92% calcite, 8% quartz), maximum Size 19 mm (3/4 in.); ASTM Type III cement, 297 kg/m³ (500 lb/cu yd); cured 2 days in mold and 6 days in fog at 22° C; loaded and exposed to drying at 8 days of age; compression stress ≈ 1/4 of 8-day strength; E = 25,500 N/mm² (3,700,000 psi); measured h in axis of cylinder is indicated in figure. Fits for f'_t = 3.45 N/mm² (500 psi), S_1 = 1.79 N/mm² (260 psi), S_0 = 0.0011, C_0 = 0.206 cm²/day (0.032 sq in./day), B = 0.]

The most important test data available in the literature on the effect of humidity have been fitted using the foregoing material parameters. The fits are drawn by curves (solid and dashed) in Figs. 4-9. The corresponding numerical values of the material parameters not yet specified appear in the captions and in Table 1. Note that all fits are shown in logarithmic time scale spanning over several orders of magnitudes. (Such fits are much more difficult to obtain than those in the actual time scale, in which eventual misfit for both too short and too long times is obscured.)

The distribution of stresses within the shrinkage and drying creep specimens have been computed for some of the data and are plotted in Fig. 10. Realistic estimates of shrinkage stresses are thus being achieved, apparently for the first

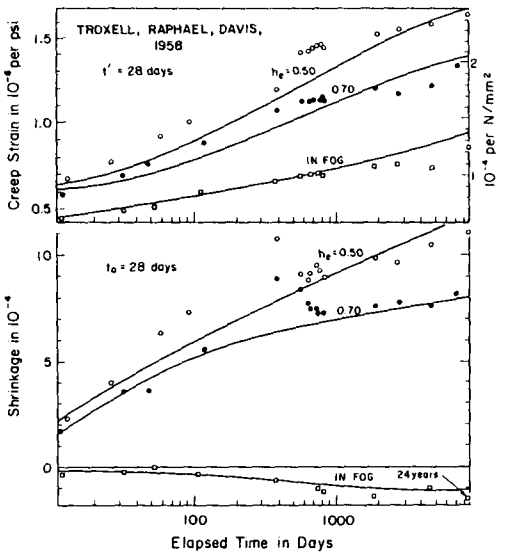

FIG. 7.—Fits of Creep and Shrinkage Data of Troxell, Raphael, and Davis (30) [Unsealed Cylinders, Diameter 102 mm (4 in.), Length 356 mm (14 in.); 28-day Cylinder Strength ≈ 17.2 N/mm² (2,500 psi), Stress = 1/3 Strength; 22° C; ASTM Cement Type I; Water-Cement-Aggregate Ratio 0.59: 1.5 : 5.67; Granite Aggregate, Maximum Size 38 mm (1.5 in.). Fits for f'_t = 2.76 N/mm² (400 psi); S_1 = 2.07 N/mm² (300 psi); S_0 = 0.008; C_0 = 1.61 cm²/day (0.025 sq in./day), B = 0.4.]

time with a constitutive law consistent with all basic material phenomena known at present.

Examination of Material Parameters and Fits of Data

1. Functions ϕ_μ in Eqs. 10-12 account for the fact that specimens that have dried up to a uniform and time-constant pore humidity h creep less for a lower h (14,16,23,28,29,34) (see Fig. 2). Functions ϕ_μ, as well as Eq. 15, are conveniently given as exponentials; the exponents of 10 approximately indicate the distance of the shift of the response function to the left in the logarithmic

time scale. [In specimens in which the drying process is well advanced but equilibrium between macropores and micropores has not yet been reached, a more complicated dependence on water loss Δw of the specimen is obtained (see Fig. 9).]

2. Functions ψ_μ^V and ψ_μ^D reflect the fact that simultaneous drying accelerates creep. (This acceleration is so strong that for normal cross-sectional dimensions it overrides ϕ_μ.) The equilibrium value of stress in water, σ_μ^h is reduced when h drops, magnifying the rate coefficients, ψ_μ^V, ψ_μ^D (Eq. 13). Since σ_μ^h is a scalar, it can appear only in combination with $\sigma_{w_\mu}^V$, and not with $\underset{\sim}{\sigma}_{w_\mu}^D$. The squares

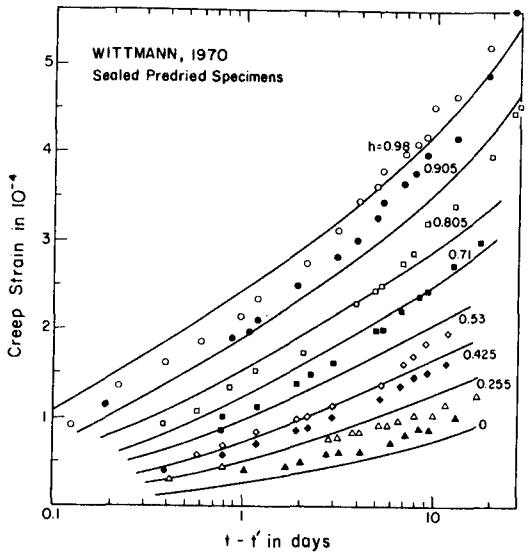

FIG. 8.—Fits of Wittmann's Data (34) on Creep at Various Constant Water Contents [Solid Cement Paste Cylinders, Diameter 18 mm, Length 60 mm; Water-Cement Ratio 0.4; Cured in Water for 28 days at 20° C, Then Dried in Oven at 105° C for 2 days; Resaturated for 3 months at Various Constant Humidities h Shown, at 20° C. Then Tested at Constant h under Stress 15.3 N/mm² (≈0.2 of Failure Stress). E ≈ 21,400 N/mm² fr 1 min Test Duration. Strain at 1 hr Creep Duration is Subtracted from All Values Shown. Fits for S_1 = 1.655 N/mm² (240 psi), S_0 = 0.004, C_0 = 0.161 cm²/day (0.025 sq in./day), B = 0.4.]

in Eq. 13 cause nonlinear dependence of drying creep upon $\sigma_{w_\mu}^V$, and thus indirectly upon σ. Thermodynamically, squares must appear here because the diffusion fluxes in the hindered adsorbed layers can depend only on an invariant, i.e., a square, of the gradient vector of the potential causing diffusion. This dependence reflects the excitation of the solid molecules when hit by the diffusing water molecules (4). The imparted energy increases the probability that the solid molecule may later jump over its activation energy barrier into an adjacent equilibrium position as a result of thermal fluctuations in energies. Since thermal movements are randomly oriented, the direction of the jumps is independent of the direction of the impinging molecule but depends on the gradient of the

TABLE 1.—Creep Compliance Values According to Fig. 13, in 10^{-7} mm²/N, as Used in Fits

Data (1)	L'Hermite, et al. (2)	Hansen and Mattock (3)	Troxell, et al. (4)	Wittman (5)
J_1	340	356	478	400
J_2	529	435	942	1,015
J_3	833	1,044	1,667	2,320
J_4	268	290	391	406
J_5	362	340	725	580
J_6	609	580	1,247	1,450
J_7	159	261	290	145
J_8	177	276	348	304
J_9	200	333	449	1,015
t', in days	7	8	7	3
	28	100	28	10
	10^4	10^4	10^4	10^4
$(t - t')$, in days	10^{-3}	10^{-3}	10^{-3}	10^{-3}
	32	32	32	1
	10^4	10^4	10^4	10^4

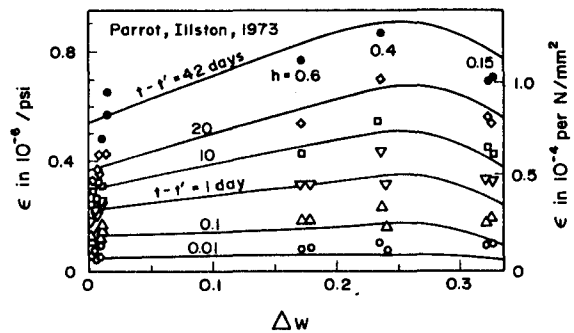

FIG. 9.—Fit of Parrot and Illston's Data (25) on Drying Creep [Hardened cement paste slabs 150 mm × 150 mm × 20 mm, water-cement ratio 0.47. Strength on 9.5 mm × 9.5 mm × 20 mm prisms was about 26.1 N/mm² (3,870 psi) (reached in 15 min). Wet cured for 7 days, then either sealed or dried in vacuum to given h for 14 days and then sealed. Loaded by uniaxial stress 8.89 N/mm² (1,290 psi) at 28 days of age. Fits are shown for f_t' = 2.76 N/mm² (600 psi), S_1 = 1.38 N/mm² (200 psi), S_0 = 0.0003, C_0 = 0.203 cm²/day (0.032 sq in./day), B_μ = 0.8 + 0.2 (μ − 1); Δw = volume of water lost per unit volume of paste, assumed proportional to (1 − h); final h values in sealed specimens were estimated as 0.98, 0.6, 0.4, 0.15, as indicated.]

potential of solids because this gradient reduces the activation energy barrier in the direction of gradient. This explains why the nonlinear diffusion effects intervene in rate coefficient $\phi^V_{ss_\mu}$ and $\phi^D_{ss_\mu}$ for solids diffusion (4).

3. Coefficients $\phi^V_{sw_\mu}$ and $\phi^D_{sw_\mu}$ reflect a different, linear type of coupling of the diffusions. They express a drag of the diffusing water molecules upon

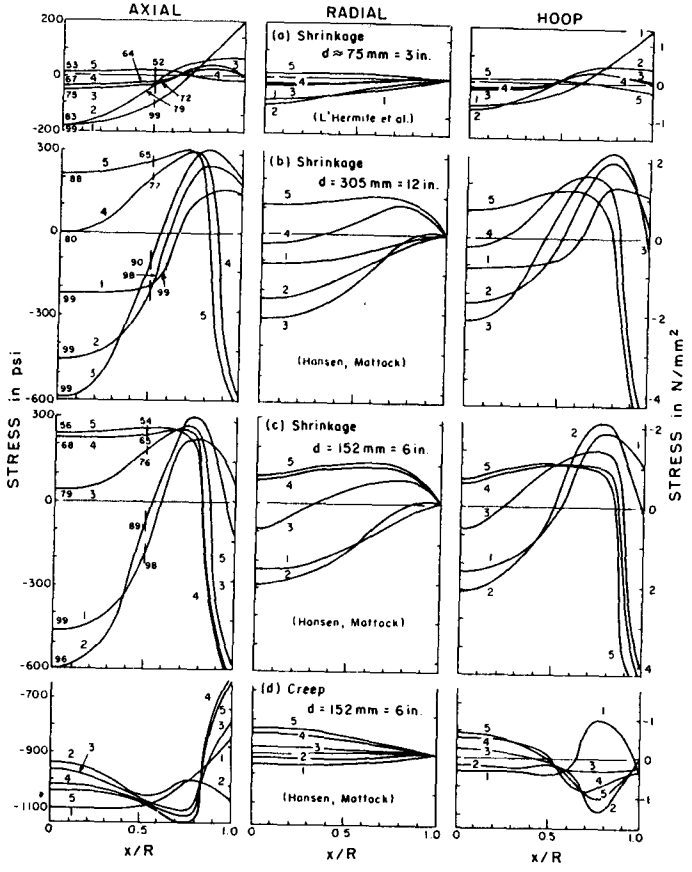

FIG. 10.—Computed Stress Distribution in Cylinders at Various Times Due to Shrnkage and Drying Creep [(*a*) Computed from Fits of Data in Figs. 4 and 5; (*b*) Computed from Fits in Fig. 6; x = Radius Coordinate; R = Radius; d = Diameter. Times from Start of Shrinkage or Creep: Case a, Curve 1–1 day, Curve 2–15 days, Curve 3—37 days, Curve 4—130 days, Curve 5—1,030 days; Cases b–d, Curve 1—5 days, Curve 2—22 days, Curve 3—100 days, Curve 4—464 days, Curve 5—2,150 days. Two-Digit Numbers Indicate Computed Humidity at x = 0 or x = R/2, as percentage]

the molecules of solids (probably CA-ions) that arise as the solid molecules are directly knocked out of their equilibrium positions by the impinging water molecules (4). The jumps then occur, in contrast with the previous case, in the direction of the gradient of water potential (rather than solids potential). They must be much less frequent than the previous type of jumps because

they require more energy, as the thermal fluctuations do not help to overcome the energy barrier. Therefore, off-diagonal coefficients $\phi^V_{sw_\mu}$, ... should be relatively small (4), which explains Eq. 12. (Furthermore, if they were not small, their effect would in many cases, e.g., compression creep, shear creep, and bending creep, offset the acceleration of creep due to $\phi^V_{ss_\mu}$, $\phi^V_{ss_\mu}$, which does not correspond to fact.)

4. Coefficient 1.2 in Eq. 16 causes the acceleration of creep by drying to be more pronounced in volumetric than in deviatoric deformations. This accounts for the fact that at simultaneous drying the apparent Poisson ratio for uniaxial creep drops with time [becoming as low as 0.05; (see Ref. 24, p. 23)] and the lateral creep is little affected by drying (22) (see Fig. 11). In terms of creep mechanism, this probably corresponds to the fact that the increase of diffusion rate due to drying in hindered adsorbed layers of one orientation should not affect much the diffusion rate in layers of another orientation. (The Poisson ratio is thus zero for the effects of drying.)

5. Functions ρ^V_μ and ρ^D_μ express the progressively nonlinear dependence of creep upon stress at higher stress levels. Note that the stress appears in Eq. 14 only in the form of tensor invariants, which guarantees that incremental (tangent) moduli exhibit isotropy. (At very high stress near failure this condition need not be met because of extensive stress-induced microcracking of one prevalent orientation.) Also, the increase in Poisson ratio near failure stress in the uniaxial tests cannot be modeled by Eq. 14 because it is known to be caused by microcracking and to be accompanied by a development of anisotropy. Instead, choosing $\rho^V_\mu = \rho^D_\mu$, no direct dependence of Poisson ratio upon stress is assumed.

6. Functions ϕ_μ and ψ^V_μ, ψ^D_μ depend on τ_μ (or μ) because the intensity of the influences of pore humidity and of drying varies with creep duration.

7. The components of delayed shrinkage of various magnitudes of the delay with regard to a change in pore humidity (the shrinkage delay spectrum) are about equally large for all delays $\tau_\mu < 20$ days and become negligible for $\tau_\mu > 20$ days. This is modeled by Eq. 19 for σ^h_μ. Term h^{200} in the humidity dependence allows one to model the large difference in shrinkage between sealed specimens and specimens in water. Eqs. 18 and 19 predict swelling in water to be about 20% and (autogeneous) shrinkage of sealed specimens to be about 5% of the maximum shrinkage. The age dependence of delayed shrinkage (clearly apparent in Ref. 20) is partly caused by the age dependence of E_μ (Eq. 21), and more by that of C (see item 11 following).

8. Coefficients 0.1 and 0.9 in Eq. 20 correspond to the assumption that the ratio of transverse stiffness of water and solids in the hindered adsorbed layers (or the ratio of spring constants in Fig. 1) is large, being taken as 9:1. This assumption was confirmed by data fitting and also appears reasonable realizing that the bulk modulus of water is much less than that of cement paste (6). As an implication of this fact, and in contrast with widespread opinion (26,27), hindered adsorbed water does not play a major role in resisting the externally applied load (6). Nevertheless, it does introduce large forces into the material, due to the term, σ^h_μ [representing a resultant of disjoining pressures (4)]. Furthermore, coefficient 0.1 in Eq. 20 also models the mild decrease of elastic modulus when h drops, as indicated by tests (23,28,35). (By contrast, some other tests indicate an increase, but this is probably merely due to the

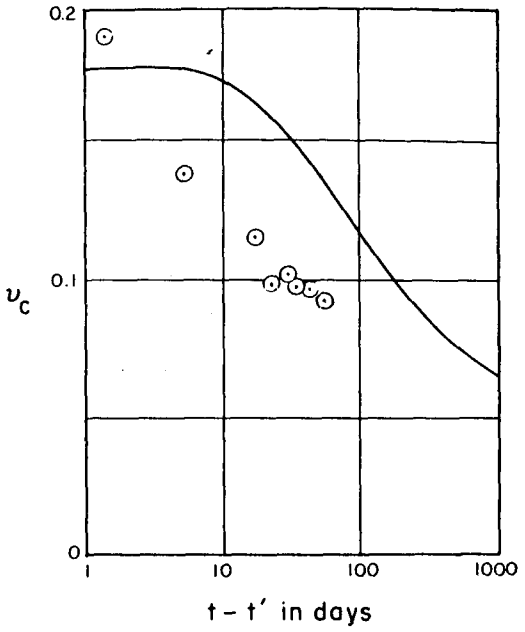

FIG. 11.—Comparison of Creep Poisson Ratios [Data Points Determined from Meyer's Data (22); Curve According to Fits of Data of Ref. 20 in Fig. 4. (Fit by Present Theory Is Not Attempted Because of Insufficient Data.) Specimens 40 cm × 40 cm × 6 cm, Drying at 65% Humidity and 20° C after Unmolding, 23 days Old at Loading; 28-day Cube Strength 350 kp/cm²; Stress ≈ 0.3 Strength; Water-Cement Ratio 0.7; 300 kg cement/m³; Maximum Gravel Size 7 mm.]

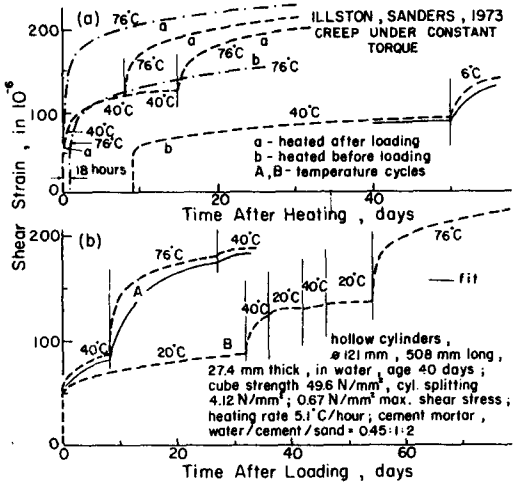

FIG. 12.—Tests of Illston and Sanders (19) on Creep at Variable Temperature

lack of separation of the short-time creep, which is smaller at lower values of h.) Eq. 20 gives a small decrease in E with h through the high h region, in which the large pores are being emptied, and a larger decrease through the low h region, in which the narrowest pores, with firmly held water capable of resisting higher stress, are being emptied.

9. Coefficient β_h in Eq. 23 interprets the diminution of the hydration rate (and thus also the rate of aging) as humidity h drops. Eq. 23 is confirmed by fitting the present data and also agrees (21,33) with more direct observations (including the fact that portland cement cannot be stores permanently at humidities above 50%).

10. The assumptions regarding the tensile behavior, though unimportant for creep data, affect appreciably the early shape of the shrinkage curves (Fig. 6), and even more the magnitude of shrinkage stresses (Fig. 10). The tensile stress-strain diagram of a small element of a nonhomogeneous material, e.g., concrete, depends on the degree of restraint and the tensile zone size. While without restraint the tensile behavior is usually brittle, with a linear σ-ϵ diagram ended by a sudden appearance of a macroscopic crack, a restrained concrete may exhibit considerable tensile ductility due to gradual microcracking (as is exemplified best by the behavior of ferrocement). The peaks of shrinkage stresses, self-equilibrated within the cross section, are usually localized and the adjacent concrete provides a restraint. This is the reason for using a curved tensile stress-strain diagram, as given by Eq. 24. The failure stress, f_t', is considered, for the same reason, equal to the tensile strength in bending (modulus of rupture f_r'), which is higher than the direct tensile strength. Under these assumptions, the stress analysis predicts no macroscopic cracks to form in the tests shown in Figs. 4-7. Indeed, no such cracks have been reported. (However, if the tensile behavior were assumed to be linear and brittle, the analyses would predict macroscopic cracks to form.) Also, no extensive cracking, except for microscopic bond cracks, is revealed by micrographs of ordinary drying concretes (18). Moreover, if macroscopic cracks were produced by shrinkage, the tensile strengths of wet specimens and of drying specimens would have to differ substantially, which is not found in reality.

11. The humidity dependence of diffusivity C (Eq. 25), determined in Ref. 7, largely controls the shape of the shrinkage curves, while the age dependence of C_1 (Eq. 26) is important for the age effect upon shrinkage (Fig. 5). Reference diffusivity C_0 was adjusted, in the case of Fig. 6, to optimize the fit of the h values in the core, which have been, fortunately, also reported for these data (17).

12. An interesting feature of stresses induced by shrinkage is the large tension that may appear in the core of the specimens after a long period of drying (Fig. 10). This is obviously due to the fact that the core is drying and shrinking relatively late, after the compression stresses previously induced in the core have been largely reduced by creep and after the surface region has already shrunken and dried up, thus, diminishing its own capability to further deform by creep. Note that the stresses due to drying creep (never before studied) are appreciable, though smaller than the shrinkage stresses (Fig. 10). The latter are highest for diameters over 15 cm (6 in.).

13. The functions of h and t_e in Eqs. 10-23 should be considered to be only approximate, e.g., replacing $\sqrt{1-h}$ in Eq. 13 with a more complicated function

can yield a closer fit of certain particular data (those in Fig. 8), or eliminate the vertical tangent of function $\sqrt{1-h}$ at $h = 1$. But at the present level of experimental information such refinements seem unnecessary.

Extension to Variable Temperature

To extend the present formulation to variable temperature, it is necessary to include instantaneous thermal dilatations into Eq. 1 (4) and consider a number of other effects:

1. All rate coefficients $\phi^V_{ss_\mu}$, $\phi^D_{ss_\mu}$, ..., depend on temperature and the expressions given previously in Eqs. 10 and 11 must be multiplied by the coefficients (4):

$$\phi_T = \exp\left[\frac{U_\mu}{R}\left(\frac{1}{T_0} - \frac{1}{T}\right)\right] \quad \ldots\ldots\ldots\ldots\ldots\ldots\ldots\ldots \quad (28)$$

in which U_μ = activation energies of creep, analyzed in Ref. 10 (for the case $h = 1$); T = absolute temperature; and R = gas constant.

2. Coefficient β_h in Eq. 23 must be multiplied by a temperature-dependent coefficient (see Refs. 4 and 10), which reflects the acceleration of the hydration rate.

3. The values, σ^h_μ, of hidden stresses in thermodynamic equilibrium also depend on temperature.

4. In calculating pore humidities h, one must consider that diffusivity C depends on T (see Ref. 7), include the change in h due to temperature change at constant water content, as given by the hygrothermic coefficient, κ, (see Ref. 7) and eventually also consider the temperature change due to latent heat of adsorption.

5. Finally, above 100° C, loading of the solid skeleton by the pressure of steam in the pores must be considered.

Effects 1 and 2 were analyzed in detail in Ref. 10, and effect 4 was analyzed in Ref. 7. Effect 3 may be approximately expressed by adding to the expression for σ^h_μ in Eq. 19 the term

$$\sigma^T_\mu = p_\mu(\bar{S}^B_w - \bar{S}_w)(T - T_0)\,h \quad \ldots\ldots\ldots\ldots\ldots\ldots\ldots\ldots \quad (29)$$

in which T_0 = initial value of T at which the material was in thermodynamic equilibrium; p_μ = positive constants (perhaps all equal); $\bar{S}^B_w$, $\bar{S}_w$ = the entropy densities of capillary water and of hindered adsorbed water, respectively (see Ref. 4, Eqs. 4.24 and 4.29). Because the two entropies are different, warming (or cooling) produces a difference in chemical potentials between hindered adsorbed water and capillary water and sets off a flow out of (or into) the hindered adsorbed layers. This flow is responsible for delayed recovery of a part of thermal dilatation and, in addition, strongly accelerates creep, because of the nonlinear diffusion coupling, reflected by the squared terms with σ^h_μ in Eq. 13 (the terms that also account for the drying creep effect). This acceleration of creep, which will be called hygrothermic, is best demonstrated by the tests (19) of Illston and Sanders (Fig. 12), who call it transitional thermal creep. These tests were performed on saturated specimens, in which the acceleration

is not complicated by effect 4 (because $\kappa = 0$ at $h = 1$).

Because σ^h_μ occurs in a squared term (in Eq. 13), acceleration occurs for both warming and cooling (as is the confirmed by the 6° C curve in Fig. 12), just as it does for both drying and wetting. The hygrothermic acceleration of creep lasts until the thermodynamic equilibrium (equality of chemical potentials) is restored and has physically the same source as the acceleration of creep due to drying. But it is generally of shorter duration and begins with a shorter lag behind the environmental humidity change because temperature change inside the specimen occurs faster than humidity change and a uniform temperature is reached earlier. The hygrothermic acceleration of creep (effect 3) is probably negligible when temperature change is slow, as in the core of massive cross sections. Similarly, as in drying creep, most (but not all) of the creep due to hygrothermic acceleration must be irrecoverable upon unloading (which agrees with the findings in Ref. 19).

An interesting property revealed by Illston and Sanders (Fig. 12) was the absence of further hygrothermic acceleration of creep upon temperature reversal (see curves A and B in Fig. 12). This can be explained by the relatively short period elapsed from the previous temperature change. Although uniform temperature has long been reached, it appears from the equations obtained herein by fitting test data at variable humidity that the thermodynamic equilibrium of the diffusion between macropores and micropores could not have been reached yet in Fig. 12 at the time of the reversal. Probably, by the time of the reversal, the difference, $\sigma^V_{w_\mu} - \sigma^h_\mu$, under square in Eq. 13 has only been reduced by the diffusion processes to about one-half. Thus, upon temperature reversal, a difference of equal value and opposite sign must have been created and, when squared, no change of the rate in Eq. 13 was thus produced. Due to the limited scope of data, all relevant parameters of the present model cannot be determined from Fig. 12. Nevertheless, it has been checked that an acceptable fit (solid line in Fig. 12) is obtained with the parameters: $n = 3$, $G_1 = 6{,}700$ N/mm², $G_2 = G_3 = G_1/2$, $\tau_1 = 10$ days, $\tau_2 = 10\,\tau_1$, $\tau_3 = 100\,\tau_1$, $T_0 = 40°$ C, $U_\mu = 5{,}000$ cal, $p_\mu(\bar{S}^b_w - \bar{S}_w) = 0.21$ N/mm² per degree Celsius, aging being neglected.

Computation of Strain and Stress Histories for Specified Material Parameters

All data considered herein, except for those in Figs. 8, 9, and 12, pertain to specimens that have been in a nonuniform state in the course of the test. Therefore, a numerical program is required for computing the stress and strain histories for any specified values of material parameters. Such a program has been written for a long hollow cylinder the cross sections of which may be assumed to be all in the same axisymmetric state and undergo the same history. The program allows for any history of loading by axial force, a torque, and internal and external pressures, as well as for prescribed displacements. Exterior or interior surface may be either sealed or exposed to air of given humidity history. As a special case, the program solves a solid cylinder. Specifying internal radius to be much larger than the wall thickness, it also solves a flat slab.

The program has been developed by extending the program used in Ref. 2. The radius coordinate, x, the only space dimension, is subdivided into a number of finite elements with constant strain. Because the cylinder is considered

long, the longitudinal strain, ϵ_z, is the same in all elements. The integration in time is carried out step-by-step. In each step, prior to stress and strain analysis, the humidity distribution at time t_r is calculated using a Crank-Nicholson type algorithm (7).

At the beginning of computation, the time steps, $\Delta t = t_r - t_{r-1}$ ($r = 2, 3, \ldots$), should be less than the shortest relaxation time considered and, to allow reaching the long-term response, they must later be increased, usually in a geometric progression. [Sufficient accuracy is achieved with $t_r - t_0 = 10^{1/4}(t_{r-1} - t_0)$.] If the standard step-by-step algorithms were applied, the time stops could not be increased arbitrarily without causing numerical instability. However each step exactly, assuming all material parameters (i.e., $\phi^V_{ss_\mu}, \ldots, G_{s_\mu}, \ldots$), as well as $\dot{\epsilon}$, $\dot{\epsilon}_S$, to be constant during the time step. An algorithm corresponding to such an exact integral is given by Eqs. 5.19-5.21 in Ref. 4. For the special case defined by Eq. 12 the exact integral considerably simplifies because Eqs. 1 split into two independent linear differential equations with constant coefficients. In this case, the exact integral of Eq. 1 can be put, after some manipulations, into the form:

$$\Delta\sigma^V_r = 3K''(\Delta\epsilon^V_r - \Delta\epsilon^{V\prime\prime}_r) \quad (30)$$

$$\Delta\sigma^V_{s_{\mu_r}} = 3K^s_\mu(\Delta\epsilon^V - \Delta\epsilon_S)\lambda^V_{s_\mu} - (1 - e^{-\phi^V_{ss_\mu}\Delta t})\sigma^V_{s_{\mu_{r-1}}} \quad (31)$$

$$\Delta\sigma^V_{w_{\mu_r}} = 3K^w_\mu(\Delta\epsilon^V - \Delta\epsilon_S)\lambda^V_{w_\mu} - (1 - e^{-\phi^V_{ww_\mu}\Delta t})\sigma^V_{w_{\mu_{r-1}}} + \lambda^V_{w_\mu}\phi^V_{ww_\mu}\sigma^h_\mu\Delta t \quad (32)$$

in which $$K'' = \sum_\mu (\lambda^V_{s_\mu} K^s_\mu + \lambda^V_{w_\mu} K^w_\mu) \quad (33)$$

$$3K''\Delta\epsilon^{V\prime\prime}_r = \sum_\mu (1 - e^{-\phi^V_{ss_\mu}\Delta t})\sigma_{s_{\mu_{r-1}}} + \sum_\mu (1 - e^{-\phi^V_{ww_\mu}\Delta t})\sigma_{w_{\mu_{r-1}}}$$

$$- \Delta t \sum_\mu \lambda^V_{w_\mu}\phi^V_{ww_\mu}\sigma^h_\mu + 3K''\Delta\epsilon_S \quad (34)$$

and in which

$$\lambda^V_{s_\mu} = \frac{1 - e^{-\phi^V_{ss_\mu}\Delta t}}{\phi^V_{ss_\mu}\Delta t}; \quad \lambda^V_{w_\mu} = \frac{1 - e^{-\phi^V_{ww_\mu}\Delta t}}{\phi^V_{ww_\mu}\Delta t} \quad (35)$$

Subscripts r refer to discrete times t_r ($r = 1, 2, \ldots$), e.g., $\sigma^V_{s_{\mu r}} = \sigma^V_{s_\mu}(t_r)$; and Δ refers to an increment over time step $\Delta t = t_r - t_{r-1}$, e.g., $\Delta\epsilon^V_r = \epsilon^V_r(t_r) - \epsilon^V_r(t_{r-1})$. Equations that result from Eq. 3 for the deviatoric components have the same form, which is obtained from Eqs. 30-35 by deleting $\Delta\epsilon_S$ and σ^h_μ, and replacing $3K''$ with $2G''$, $3K^s_\mu$ with $2G^s_\mu$, $\Delta\sigma^V_r$ with $\Delta\sigma^D_{ij_r}$, etc. Unconditional numerical stability can be proven for the preceding formulas in the same way as for those in Ref. 9 and was also confirmed by computational experience.

Eq. 30 has the form of an elastic stress-strain relation with modulus K'' and inelastic strain $\Delta\epsilon^{V\prime\prime}_r$, and so the solution $\Delta\underset{\sim}{\epsilon}_r$, $\Delta\underset{\sim}{\epsilon}_r$ in any time step is a linear elasticity problem with inelastic strains, the handling of which by the finite element method is well known. After solving $\Delta\underset{\sim}{\epsilon}_r$, the hidden stresses at t_r can be determined from Eqs. 31 and 32. Because of the nonlinearity of Eqs. 1-4, solution of each step Δt is iterated twice. In the first computation, all material parameters dependent on stresses ($\phi^V_{ss_\mu}, \ldots, K^s_\mu, \ldots$) are evaluated

for the stress values at the beginning of time step t_{r-1}. In the subsequent iteration (aimed at improving the values of $\underset{\sim}{\epsilon}_r$, $\underset{\sim}{\epsilon}_{s_{\mu r}}$, $\underset{\sim}{\epsilon}_{w_{\mu r}}$), they are evaluated for the stress values obtained for the midstep, $(t_{r-1} + t_r)/2$, in the previous computation. All time-variable coefficients independent of stresses are always evaluated for the midstep.

When the program subroutine for the analysis of a cylinder by time steps and spatial finite elements is hooked on the optimization algorithm described in the sequel, the subroutine has to be run a great number of times. This had made the computations (on CDC-6400) very expensive, even though the problem involves only one space dimension. Therefore, no analyses with two or three space dimensions have been carried out.

The finite length cylinders used as test specimens have been approximated as long cylinders, in which all cross sections must remain plane. In the case of drying, this is probably quite acceptable when the ends of test cylinders are sealed (the case in Fig. 6), so at least the humidity distributions, if not the stress distributions, are to be exactly the same in all cross sections. When the ends are exposed, a more pronounced difference in shrinkage between the axis of the specimen and its surface is observed (20) in the tests (unless the gage length would be very small and the specimen very long, which was not the case in Ref. 20). In evaluating such test data (Fig. 5), the value of shrinkage (20) in the axis (rather than on the surface was assumed to be closer to that of a long cylinder and was used in data fitting. The tests (Figs. 4 and 5) that were carried out on square prisms were approximated for data fitting as cylinders of a diameter that gives about the same rate of drying, according to the charts in Ref. 7. (It does not equal the diameter that gives the same volume-to-surface ratio.)

Because of the nonlinearity of Eqs. 1-4, creep and shrinkage are not additive. Therefore, to obtain the strains and stresses due to loading alone (representing the elastic solution plus creep), the program computes first the solution due to loading and drying combined, then the solution due to drying alone, and finally subtracts the latter from the former, as is actually done in measurements.

Identification of Material Parameters from Test Data by Optimization Methods

Behavior of the test specimens is described by a differential equation in space and time, the coefficients of which are unknown and must be determined from prescribed solutions, the given data. This represents an inverse (initial-boundary value) problem, a typical problem of control theory. Such problems are presently receiving vivid attention from the mathematicians and various optimization techniques have been developed to tackle them (12). One of them is the method of quasilinearization (12,13) the discrete version of which has been applied to the present problem. Although it has been already described in Ref. 10, it needs to be outlined herein briefly, as a background to further considerations.

The measured creep or shrinkage curves are represented by discrete characteristic data points, $\bar{F}_\alpha$ ($\alpha = 1, 2, \ldots, N_\alpha$), which must be uniformly distributed over the region of interest. (For example, they should be uniformly spaced in the logarithmic time scale.) Let $F_\alpha(p_m)$ = the theoretical solution for the same times and locations as $\bar{F}_\alpha$, furnished by the program described previously. Assume $F_\alpha(p_m)$ to be a smooth function of unknown material parameters p_m

($m = 1, 2, \ldots, N_m$) fed into the program. Further assume that a certain sufficiently good estimate, p_m^0, of the unknown material parameters has been obtained by the trial-and-error approach coupled with intuition. The solution depends nonlinearly upon p_m, but for p_m sufficiently close to p_m^0 this dependence may be linearized. To this end, partial derivatives $F_{\alpha,k}$ of F_α with regard to p_k are needed. Computing the solutions for parameters $p_m^0 + \delta_{mk}\Delta p_k$, (in which Δp_k = a chosen very small increment; and $\delta_{mk} = 0$ for $m \neq k$ and $\delta_{mk} = 1$ for $m = k$) derivatives $F_{\alpha,k}$ may be approximated as

$$F_{\alpha,k} \approx \frac{F_\alpha(p_m^0 + \delta_{mk}\Delta p_k) - F_\alpha(p_m^0)}{\Delta p_k} \quad \ldots\ldots\ldots\ldots\ldots\ldots \quad (36)$$

Then, noting that $F_\alpha(p_m) \approx F_\alpha(p_m^0) + F_{\alpha,k}(p_k - p_k^0)$, the objective of optimum fit may be achieved by imposing the least-square condition

$$\Phi = \sum_\alpha w_\alpha \left[F_\alpha(p_m^0) + \sum_k F_{\alpha,k}^0 (p_k - p_k^0) - \tilde{F}_\alpha \right]^2 + \Phi_1 = \text{minimum} \quad \ldots \quad (37)$$

in which w_α = suitably chosen weights; Φ_1 = chosen quadratic penalty term (if any), which may express certain smoothing condition or constraint, or include terms of the type $(p_m - p_m^0)^2$ to prevent unreasonably large change $(p_m - p_m^0)$. The minimizing conditions, $\partial\Phi/\partial p_j = 0$, yield a system of linear algebraic equations

$$\sum_m A_{jm}(p_m - p_m^0) = B_j; \quad j, m = 1, 2, \ldots, N_m \quad \ldots\ldots\ldots\ldots\ldots \quad (38)$$

$$\text{with} \quad A_{jm} = \sum_\alpha w_\alpha F_{\alpha,j} F_{\alpha,m} + A'_{jm};$$

$$b_j = \sum_\alpha w_\alpha [\tilde{F}_\alpha - F_\alpha(p_m^0)] F_{\alpha,j} + B'_j \quad \ldots\ldots\ldots\ldots\ldots\ldots \quad (39)$$

in which A'_{jm}, B'_j = the contributions from the penalty term, Φ_1. The improved values of p_m, solved from Eq. 38, may then be renamed p_m and the whole optimization procedure may be repeated in several stages. The convergence is rapid, because quasilinearization methods exhibit quadratic convergence; but it will occur only if p_m^0 are "sufficiently good" estimates. [The procedure given by Eqs. 36–39 is in fact an extension of the least-square curve fitting method of Gauss and Legendre (32)].

Another suitable optimization method for the present problem is Powell's method for a sum-of-squares nonlinear function, which does not require computation of derivatives (32). Although its rate of convergence is less, its range of convergence is much broader, so that a very good initial guess of material parameters is not requisite.

No single data set exists that would be sufficiently large for determining all material parameters for creep and shrinkage considered herein. It is, therefore, necessary to optimize simultaneously the fits of different sets of data obtained in different laboratories with different concretes. Such a simultaneous optimization can be undertaken only if a certain similarity between different concretes is assumed. (This assumption is justified, of course, because without any similarity between different concretes the term concrete, per se, would lose all meaning.)

Due to this similarity, some material parameters must exist that are the same, or nearly the same, for all concretes. While the parameters characterizing the reference creep properties (at $h = 1$) are normally different for different concretes, those that modify the reference creep properties for humidity effects can probably be assumed to be nearly the same for all concretes. Thus, e.g., the parameter that equals 3.6 in Eq. 15 is for all data sets denoted by the same p_m (say P_7), whereas coefficient S_0 in Table 1 and Eq. 18 is designated by a different p_m (e.g., P_{17}, p_{18}, p_{19}) for different data sets. Also, note that, aside from strains (or stresses), the values of pore humidity or water content, when given (Fig. 6), should be included among the data points, $\tilde{F}_\alpha$, to be fitted.

To obtain coefficients $F_{\alpha,k}$ and F_α (Eq. 36), it is obviously necessary to compute $N_m + 1$ solutions for each curve to be fitted. The program for solving the stress and strain history must be run $N_1 N_0 (N_m + 1)$ times, N_1 being the number of curves to be fitted and N_0 the number of optimization stages. Thus, the number of repetitions becomes necessarily quite large.

Looking at the data on reference creep at $h = 1$ (8,9), one may see that the uniaxial creep compliance function, $J(t, t')$, representing strain at time t

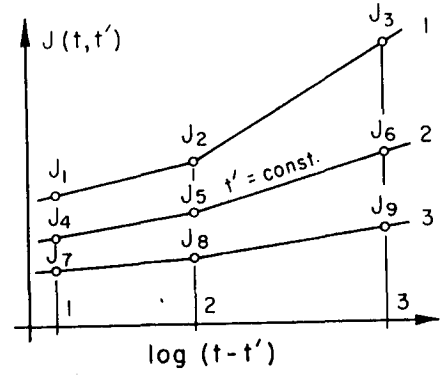

FIG. 13.—Characteristic points for Reference Creep Function $J(t, t2')$.

caused by a unit stress acting from time t', can be sufficiently characterized by nine values $J_1, \ldots, J_9$ shown in Fig. 11 (and given in Table 1). In a subroutine of the program, $J(t, t')$ for any t and t' is computed by interpolation from the four closest J values (or, beyond the extreme points, by extrapolation), assuming J to depend linearly upon $\log(t - t')$ and upon t'^{-n} with $n = 0.3 + 0.3/(1 + t - t')$. From $J(t, t')$, another subroutine then computes $E_\mu(t)$ (from Eq. 22), using an algorithm developed in Ref. 9, and listed in an improved form in Ref. 11.

For reasons of numerical instability, it is expedient to treat as material parameters the values, $J_1, \ldots, J_9$ (see Fig. 13), rather than the values, E_μ, in Eq. 22. In each data set, some of these values, e.g., $J_1, \ldots, J_5$, have directly been measured and are thus fixed in advance. Others, e.g., $J_6, \ldots, J_9$, have not been measured and must be estimated. These must be included among the unknown parameters, p_m, to be found by optimization.

To set up a general program, all material parameters that are unknown at least for some data may be included, for programmer's expedience, among

the p_m. Then, of course, for some of the simultaneously optimized data sets a certain parameter, e.g., p_i, is known in advance. Despite this, it is convenient to treat p_i as unknown, but A_{im} and B_i must then be assigned values that assure the solution of p_i to equal the known value p_i^0. This can be assured if all B_i and A_{im} for $m \neq 1, \ldots, N_m$ (Eq. 37), except A_{ii}, are set equal to 0.

Finally, it need be stressed that optimization can provide the best fit only within the limitations of the type of functions introduced in Eqs. 10-27. The choice is partly a matter of intuition, but is greatly helped by a quantitative theory of creep mechanism (3,4,6). Although a number of different functions have been tried, the functions in Eqs. 10-27 should not be regarded as the best possible choice. They are only acceptable.

Conclusions

1. The constitutive law for creep and shrinkage of concrete at variable humidity can be formulated in a rate-type form with hidden stresses, the current values of which fully characterize the past history. This fact considerably simplifies the step-by-step creep analysis.

2. The hidden stresses are of two types: (a) Those in solids; and (b) those in (hindered adsorbed) water. This separation is necessary to account: (a) For the delay of drying creep and of a substantial part of shrinkage with respect to a change in the pore humidity; and (b) for the contrast between the near linearity of creep at constant pore humidity and the distinct nonlinearity of drying creep in the working stress range.

3. While the creep parameters for constant humidity vary considerably from concrete to concrete, the ratios in which the properties are modified by humidity effects are nearly the same for all concretes. The same holds for shrinkage.

4. The success in fitting the creep and shrinkage test data for variable humidity, as well as in fitting the data for constant humidity and variable temperature (9,10), corroborates the theory based on irreversible thermodynamics from which Eqs. 1-4 were developed (4,6) and, in particular, confirms the following: (a) Drying creep and a substantial part of shrinkage are delayed with regard to the pore humidity; (b) although hindered adsorbed water (or interlayer water) introduces large forces into the solid microstructure of cement gel, it represents, in terms of elastic stiffness, a relatively soft component and receives only a small part of the externally applied load; (c) the mobility of the solids in cement gel is caused mainly by the presence of water; (d) this mobility is increased by diffusion coupling when water molecules diffuse simultaneously; and (e) this coupling between diffusions of solids and of water is nonlinear and is probably the source of the acceleration of creep by simultaneous drying.

5. In the constitutive law presented, creep and delayed shrinkage are not linearly additive and are both governed by the same hidden stresses. This reflects the identity of their physical mechanisms.

6. A realistic estimate of shrinkage stresses, as well as of stresses induced by drying creep (never before studied), has been reached (Fig. 9).

7. The step-by-step integration in time may be based on Eqs. 28-33, which allow arbitrary increase of the time step without causing numerical instability.

8. Identification of the material parameters from test data represents an inverse nonlinear initial boundary value problem that can be solved by an optimization algorithm based on a least-square condition. Simultaneous fitting of data sets for different concretes is requisite.

9. In contrast with the existing formulations of creep at variable humidity, the constitutive law presented is consistent in the continuum mechanics sense because it is tensorially invariant, does not contain the time explicitly, and includes only local material variables.

10. The law presented satisfies the requirement of compatibility with the previously established rate-type creep law at constant humidity (9) and at variable temperature (10).

11. The creep and shrinkage law of concrete at variable humidity is now available for practical applications. It is necessary in the design of special structures. For the design of ordinary structures it is too complicated, unless it could be embodied in a standard generally available program.

Acknowledgment

The present study represents a part of a project sponsored by the United States National Science Foundation under Grant GK-26030. Zissis Mosehovidis of Northwestern University is to be thanked for helping to prepare a part of the computer program.

Appendix I.—References

1. Bažant, Z. P., "Constitutive Equation for Concrete Creep and Shrinkage Based on Thermodynamics of Multiphase Systems," *Materials and Structures* Vol. 3, Paris, France, 1970, pp. 3-36; also *Report 68/1*, Department of Civil Engineering, University of Toronto, Toronto, Canada, 1968.
2. Bažant, Z. P., "Numerical Analysis of Long-Time Deformations of a Thick-Walled Concrete Cylinder," *Report No. 69-12*, Division of Structural Engineering and Structural Mechanics, University of California, Berkeley, Calif., Aug., 1969; also American Concrete Institute, *Supplement, Paper SP 27-21* Detroit, Mich.
3. Bažant, Z. P., "Thermodynamics of Interacting Continua with Surfaces and Creep Analysis of Concrete Structures," *Nuclear Engineering and Design*, Vol. 20, 1972, pp. 477-505.
4. Bažant, Z. P., "Theory of Creep and Shrinkage in Concrete Structures: A Précis of Recent Developments," *Mechanics Today*, Vol. 2 Pergamon Press, Inc., New York, N.Y., 1974, pp. 1-93.
5. Bažant, Z. P., and Asghari, A., "Computation of Age-Dependent Relaxation Spectra," *Cement and Concrete Research*, Vol. 4, 1974, pp. 567-579.
6. Bažant, Z. P., and Moschovidis, Z., "Surface Diffusion Theory for the Drying Crrep Effect in Portland Cement Paste and Concrete," *Journal of the American Ceramic Society*, Vol. 56, 1973, pp. 235-241.
7. Bažant, Z. P., and Najjar, L. J., "Nonlinear Water Diffusion in Non-Saturated Concrete," *Materials and Structures*, Vol. 5, 1972, pp. 3-20.
8. Bažant, Z. P., and Wu, S. T., "Dirichlet Series Creep Function for Aging Concrete," *Journal of the Engineering Mechanics Division*, ASCE, Vol. 99, No. EM2, Proc. Paper 9645, Apr., 1973, pp. 367-387.
9. Bažant, Z. P., and Wu, S. T., "Rate-Type Creep Law of Aging Concrete Based on Maxwell Chain," *Materials and Structures*, Vol. 7, 1974, pp. 45-60.
10. Bažant, Z. P., and Wu, S. T., "Thermoviscoelasticity of Aging Concrete," *Journal of the Engineering Mechanics Division*, ASCE, Vol. 100, No. EM3, Proc. Paper 10621, June, 1974, pp. 575-597.
11. Bažant, Z. P., et al., "A Thin-Walled Cement Paste Cylinder for Creep Tests at

Variable Temperature and Humidity," *Materials and Structures*, Vol. 6, 1973, pp. 277-281.
12. Bellman, R. E., *Methods of Nonlinear Analysis*, Vol. 2, Academic Press, New York, N.Y., 1973.
13. Bellman, R. E., and Kalaba, R. E., *Quasilinearization and Nonlinear Boundary Value Problems*, American Elsevier Publishing Co., Inc., New York, N.Y., 1965.
14. Cilosani, Z. N., "On the True Mechanism of Creep of Concrete" (in Russian), *Beton i Zhelezobeton*, Vol. 2, Moscow, U.S.S.R., 1964, pp. 75-78.
15. Fahmi, H. M., Polivka, M., and Bresler, B., "Effect of Sustained and Cyclic Elevated Temperature on Creep of Concrete," *Cement and Concrete Research*, Vol. 2, 1972, pp. 591-606.
16. Glucklich, J., and Ishai, O., "Creep Mechanisms in Cement Mortar," *Journal of the American Concrete Institute*, Vol. 59, 1962, pp. 923-948.
17. Hansen, T. C., and Mattock, A. H., "Influence of Size and Shape of Member on the Shrinkage and Creep of Concrete," *Journal of the American Concrete Institute*, Vol. 63, pp. 267-290.
18. Hsu, T. T. C., et al., "Microcracking of Plain Concrete and the Shape of the Stress-Strain Curve," *Journal of the American Concrete Institute*, Vol. 60, 1963, pp. 209-224.
19. Illston, J. M., and Sanders, P. D., "The Effect of Temperature Change upon the Creep of Mortar under Torsional Loading," *Magazine of Concrete Research*, Vol. 25, No. 84, 1973, pp. 136-166.
20. L'Hermite, R., Mamillan, R., and Lefèvre, C., "Nouveaux résultats de recherches sur la déformation et la rupture du béton," *Annales de l'Institut Technique du Bâtiment et des Travaux Publics*, No. 207-8, 1965, pp. 323-360.
21. Mamillan, M., and Lelan, M., "Le Fluage du béton," *Annales de l'Institut Technique du Bâtiment et des Travaux Publics, Supplément*, Vol. 23, No. 270, 1970, p. 12.
22. Meyer, H. G., "On the Influence of Water Content and of Drying Conditions on Lateral Creep of Plain Concrete," *Materials and Structures*, Vol. 2, No. 8, 1969, pp. 125-131.
23. Mullen, W. G., and Dolch, W. L., "Creep of Portland Cement Paste," *Proceedings*, American Society for Testing and Materials, Vol. 64, 1964, pp. 1146-1170.
24. Neville, A. M., *Creep of Concrete: Plain, Reinforced, Prestressed*, North Holland Publishing Co., Amsterdam, The Netherlands, 1970.
25. Parrott, L. J., and Illston, J. M., "Prediction of Load-Induced Dimensional Changes in Concrete," presented at the April 9-13, 1973, ASCE National Structural Engineering Meeting, held at San Francisco, Calif. (Preprint 1935).
26. Powers, T. C., "Some Observations on the Interpretation of Creep Data," *Bulletin*, Reunion Internationale des Laboratoires d'Essais et de Recherches sur les Materiaux et les Constructions, No. 33, Paris, France, Dec., 1966, pp. 381-391.
27. Powers, T. C., "Mechanism of Shrinkage and Reversible Creep of Hardened Cement Paste," *Proceedings*, September, 1965, Imperial College International Conference on the tructure of Concrete, *Paper Gl*, Cement and Concrete Association, London, England, 1968, pp. 319-344.
28. Ross, A. D., Illston, J. M., and England, G. L., "Short and Long-Term Deformations of Concrete as Influenced by Its Physical Structure and State," *Proceedings*, September, 1965, Imperial College International Conference on the Structure of Concrete, *Paper H1*, Cement and Concrete Association, London, England, 1968, pp. 407-422.
29. Ruetz, W., "The Two Different Physical Mechanisms of Creep of Concrete," *Proceedings*, September, 1965, Imperial College on the Structure of Concrete, Cement and Concrete Association, London, England, 1968, pp. 146-153.
30. Troxell, G. E., Raphael, J. M., and Davis, R. W., "Long-Time Creep and Shrinkage Tests of Plain and Reinforced Concrete," *Proceedings*, American Society for Testing and Materials, Vol. 58, 1958, pp. 1-20.
31. Wierig, H. J., "Die Wasserdampfdurchlässigkeit von Zementmörtel und Beton," *Zement-Kalk-Gips*, Nov., 1965, No. 9, pp. 471-482.
32. Wilde, D. J., and Beightler, C. S., *Foundations of Optimization*, Prentice-Hall, Inc., Englewood Cliffs, N.J., 1967, Chap. 7-06.
33. Wittman, F., "Surface Tension, Shrinkage and Strength of Hardened Cement Paste," *Materials and Structures*, Vol. 1, 1968, pp. 547-552.
34. Wittman, F., "Einfluss des Feuchtigkeitsgehaltes auf das Kriechen des des Zement-

steines," *Rheologica Acta*, Vol. 9, 1970, pp. 282-287.
35. Wittmann, F., "Bestimmung Physikalischer Eigenschaften des Zementsteins," *Deutscher Ausschuss für Stahlbeton*, Heft 232, W. Ernst und Sohn, Berlin, West Germany, 1974.

Appendix II.—Notations

The following symbols are used in this paper:

E, E_μ = Young's modulus and modulus of μth spring of Maxwell chain;
G, K = shear modulus and bulk modulus;
G^w_μ, G^s_μ, K^w_μ, K^s_μ = moduli for water and solid for μth unit of chain in Fig. 1, corresponding to K and G;
h = pore humidity (relative vapor pressure);
t, t_e = time and equivalent hydration period;
ϵ^V, $\underset{\sim}{\epsilon}^D$ = volumetric strain and deviatoric strain tensor;
ϵ_s = instantaneous shrinkage strain;
ν = Poisson ratio;
σ^V, $\underset{\sim}{\sigma}^D$ = volumetric stress and deviatoric stress tensor;
$\sigma^V_{w_\mu}$, $\sigma^V_{s_\mu}$, $\underset{\sim}{\sigma}^D_{w_\mu}$, $\underset{\sim}{\sigma}$ = stresses in water and solids in μth unit of chain in Fig. 1, corresponding to σ^V and $\underset{\sim}{\sigma}^D$;
$\phi^V_{ss_\mu}$, $\phi^V_{sw_\mu}$, $\phi^V_{ww_\mu}$, $\phi^D_{ss_\mu}$, $\phi^D_{sw_\mu}$, $\phi^D_{ww_\mu}$ = rate coefficients in Eqs. 1-4.